Distribution of oscillator strength in Gaussian quantum dots: An energy flow from center-of-mass mode to internal modes

Tokuei Sako*
Laboratory of Physics, College of Science and Technology, Nihon University, 7-24-1 Narashinodai, Funabashi, 274-8501 Chiba, Japan

Paul-Antoine Hervieux
Institut de Physique et Chimie des Matériaux de Strasbourg, GONLO, 23 Rue du Loess, 67034 Strasbourg, France

Geerd H. F. Diercksen†
Max-Planck-Institut für Astrophysik, Karl-Schwarzschild-Strasse 1, D-85741 Garching, Germany
(Received 17 April 2006; revised manuscript received 18 May 2006; published 27 July 2006)

The energy spectra and oscillator strengths of two, three, and four electrons confined by a quasi-two-dimensional attractive Gaussian-type potential have been calculated for different strength of confinement ω and potential depth D by using the quantum chemical configuration interaction (CI) method employing a Cartesian anisotropic Gaussian basis set. A substantial redshift has been observed for the transitions corresponding to the excitation into the center-of-mass mode. The oscillator strengths, concentrated exclusively in the center-of-mass excitation in the harmonic limit, are distributed among the near-lying transitions as a result of the breakdown of the generalized Kohn theorem. The distribution of the oscillator strengths is limited to the transitions located in the lower-energy region when ω is large but it extends towards the higher-energy region when ω becomes small. The analysis of the CI wave functions shows that all states in the energy range covered by the present study can be classified according to the *polyad quantum nnumber* v_p. It is shown that the distribution of the oscillator strengths for large ω occurs among transitions involving excited states with the same value of v_p as the center-of-mass excited state, $v_{p,cm}$, while it occurs among transitions involving the excited states with $v_p=v_{p,cm}$ and $v_p=v_{p,cm}+2$ for small ω.

DOI: 10.1103/PhysRevB.74.045329 PACS number(s): 71.10.Li, 31.15.Ar, 68.65.Hb, 71.15.Ap

I. INTRODUCTION

Recent advances in semiconductor technology allow the construction of quantum systems consisting of a small number of electrons confined in nanoscale potential wells, referred to as artificial atoms[1] or quantum dots.[2,3] These confined quantum systems have a certain similarity with atoms in that they have a discrete energy-level structure that follows Hund's rules.[4,5]

Quantum dots have been modeled by harmonic-oscillator potentials[2] while atoms are characterized by Coulomb potentials. The spectral properties of harmonic-oscillator quantum dots or parabolic quantum dots[6,7] are exotic as compared to those of atoms in that the oscillator strengths are concentrated only in one dipole-allowed transition. This property of harmonic-oscillator quantum dots is a direct consequence of the generalized Kohn theorem[6,8–13] and is independent of the number of electrons, the strength of the confinement, and the form of the electron-electron interaction potential.

On the other hand, it has been demonstrated recently that a realistic confining potential which can simulate experimental observations deviates from the exact harmonic-oscillator potentials.[14] In the case when the confining potential deviates from the harmonic-oscillator potential, Kohn's theorem is no longer applicable and the oscillator strengths are distributed among the transitions near the original dipole-allowed transition.[15–18] According to the generalized Kohn theorem the dipole-allowed transition in harmonic oscillator quantum dots corresponds to the excitation of a center-of-mass mode (CM) of electrons. Therefore the fragmentation of the oscillator strength among the near-lying transitions in *anharmonic* quantum dots is due to the interaction between the center-of-mass mode and internal modes of the electrons induced by the anharmonicity of the potential.

In the present study, in order to understand the interaction between the center-of-mass mode and the internal modes represented in the distribution of oscillator strengths, the spectral properties of N-electrons ($N=2$, 3, and 4) confined by a quasi-two-dimensional Gaussian potential have been studied for all spin states by using a quantum chemical multi-reference configuration interaction (CI) method employing a Cartesian anisotropic Gaussian basis set with large angular momentum functions. The computed oscillator strengths have been examined with respect to the nodal pattern in the CI wave functions for the states involved in the transitions. Atomic units are used throughout this paper.

II. COMPUTATIONAL METHODOLOGY

A. Schrödinger equation

The Schrödinger equation for N-electrons confined by a potential $\mathcal{W}$ is given by

$$[\mathcal{H}(\boldsymbol{r})+\mathcal{W}(\boldsymbol{r})]\Psi(1,2,\ldots,N)=E\Psi(1,2,\ldots,N), \quad (1)$$

where the set $(1,2,\ldots,N)$ denotes the orbital and the spin coordinates of the electrons. The operator $\mathcal{H}$ represents the N-electron operators describing the kinetic energy and the electron-electron repulsion potentials

$$\mathcal{H}(\boldsymbol{r}) = \sum_{i=1}^{N} \left[-\tfrac{1}{2}\nabla_i^2 \right] + \sum_{i>j}^{N} \left[\frac{1}{|\mathbf{r}_i - \mathbf{r}_j|} \right], \tag{2}$$

where $\boldsymbol{r} \equiv \{\boldsymbol{r}_1, \boldsymbol{r}_2, \ldots, \boldsymbol{r}_N\}$ stands for the spatial coordinates of the electrons. The N-electron interaction potential is defined as the sum of one-electron contributions

$$\mathcal{W}(\boldsymbol{r}) = \sum_{i=1}^{N} w(\boldsymbol{r}_i), \tag{3}$$

where the one-electron confining potential $w(\boldsymbol{r}_i)$ is chosen, in the present study, to be the sum of an isotropic Gaussian-type potential for the x and y directions and a harmonic-oscillator potential for the z direction

$$w(\boldsymbol{r}_i) = -D \exp[-\gamma(x_i^2 + y_i^2)] + \frac{1}{2}\omega_z^2 z_i^2, \tag{4}$$

where $\boldsymbol{r}_i = \{x_i, y_i, z_i\}$ and $D > 0$. It is noted that for sufficiently large values of ω_z the electrons of the system are strongly compressed along the z direction. Therefore in this case the system can be regarded as a quantum system confined by a two-dimensional Gaussian-type potential, i.e., as a *quasi-two-dimensional Gaussian quantum dot*. Since a Gaussian potential can be approximated close to the minimum by a harmonic-oscillator potential, the potential of Eq. (4) is suitable for modeling the confining potential of semiconductor quantum dots with anharmonicity.[19]

The anharmonicity of the Gaussian potential in Eq. (4) may be characterized by the depth of the Gaussian potential D. By taking the two leading terms of the Taylor expansion with respect to the minimum the Gaussian potential is approximated by the harmonic-oscillator potential with ω defined by

$$\omega = \sqrt{2D\gamma}. \tag{5}$$

Accordingly, the Gaussian potential may be specified by D and ω instead of D and γ. When D is much larger than ω the Gaussian potential has many bound states and the potential curve follows closely the harmonic oscillator potential with ω as illustrated schematically in Fig. 1(a) for a one-dimensional Gaussian potential. In this case the anharmonicity of the potential is small. On the other hand, when D is only slightly larger than ω the Gaussian potential has only few bound states and, therefore, deviates strongly from the harmonic-oscillator potential as illustrated in Fig. 1(b). In this case the anharmonicity is large. These observations suggest that the anharmonicity of the Gaussian potential may be defined by the parameter α, the strength of confinement over the depth of the potential as

$$\alpha = \omega/D. \tag{6}$$

The total energies and wave functions of the quasi-two-dimensional Gaussian quantum dot with the confining potential of Eq. (4) have been calculated as the eigenvalues and eigenvectors of the CI matrix. The full CI and multireference CI methods have been used for two-electron and three- and four-electron quantum dots, respectively. All calculations have been performed by using OpenMol,[20] an object-oriented program that has originated in the Molecular Physics Group of the Max-Planck-Institute for Astrophysics and is being developed in international cooperation amongst individual researchers primarily for their own use. For the study of confined quantum systems OpenMol has been extended to account for Gaussian and power-series potentials and *anisotropic* Gaussian basis functions. The electron density plots have been generated by using the gOpenMol program.[21,22] The computational results are represented in atomic units and can be scaled by the effective Bohr radius of 9.79 nm and the effective Hartree energy of 11.9 meV for GaAs semiconductor quantum dots.[23,24]

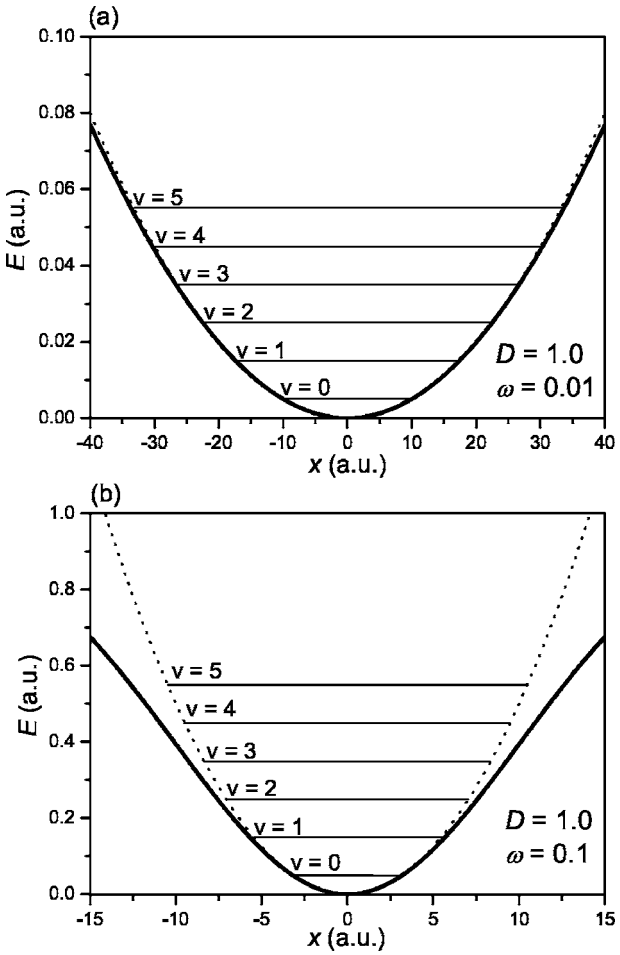

FIG. 1. One-dimensional attractive Gaussian potential with small (a) and large (b) anharmonicity. The dotted curves represent the corresponding harmonic oscillator potential with ω defined by Eq. (5). The origin of the energy axis is chosen to coincide with the minimum of the Gaussian potential.

B. Basis set

In previous studies of this series[25–27] it has been demonstrated that a set of properly chosen Cartesian anisotropic Gaussian-type orbitals (c-aniGTOs) is the most convenient choice to correctly approximate the wave function of electrons confined by an anisotropic harmonic oscillator potential. Therefore it is most natural to explore first the suitability

of a c-aniGTO basis set for expanding the wave function of electrons confined by the potential of Eq. (4). Since a c-aniGTO basis set can be transformed into a set of eigenfunctions of the corresponding anisotropic harmonic oscillator,[27] it should be also useful in the studies of atoms in strong magnetic fields[28,29] and of semiconductor quantum dots[30,31] for calculating eigenvalues and eigenfunctions with high accuracy.[32–34]

A Cartesian anisotropic Gaussian-type orbital centered at (b_x,b_y,b_z) is defined by

$$\chi_{ani}^{\vec{a},\vec{\zeta}}(\vec{r};\vec{b}) = x_{b_x}^{a_x} y_{b_y}^{a_y} z_{b_z}^{a_z} \exp(-\zeta_x x_{b_x}^2 - \zeta_y y_{b_y}^2 - \zeta_z z_{b_z}^2), \qquad (7)$$

where $x_{b_x}=(x-b_x)$, etc. Following the quantum chemical convention the orbitals are classified as s-type, p-type, … for $a=a_x+a_y+a_z=0,1,\ldots$, respectively. The (b_x,b_y,b_z) parameters have been chosen to coincide with the center of the confining potential of Eq. (4), i.e., the origin of the Cartesian coordinate system. The optimal orbital exponents $(\zeta_x,\zeta_y,\zeta_z)$ for approximating wave functions of electrons confined by an anisotropic harmonic oscillator potential have been found to be half the strength of confinement, i.e., $(\omega_x/2,\omega_y/2,\omega_z/2)$.[27] Since a two-dimensional isotropic Gaussian potential can be approximated near its minimum by the two-dimensional isotropic harmonic oscillator potential with $\omega(=\omega_x=\omega_y)$ defined by Eq. (5) it is reasonable to choose half of ω as a first approximation for the optimal Gaussian orbital exponents.

However, as discussed in the previous section, the quadratic approximation of the Gaussian potential is valid only if the anharmonicity α of the Gaussian potential is rather small. If the Gaussian potential is strongly anharmonic the harmonic oscillator potential with ω defined by Eq. (5) is too localized as compared to the Gaussian potential as shown in Fig. 1(b). Consequently, in this case the eigenfunctions of the harmonic oscillator potential cannot properly span the one-electron space of the wave function of electrons in a Gaussian potential even for the low-lying states.

One way to overcome this difficulty is to adopt a smaller ω than that defined by Eq. (5) so that the harmonic oscillator eigenfunctions cover properly the space defined by the Gaussian potential. An ω (which will be denoted by $\tilde{\omega}$) appropriate for a given Gaussian potential may be determined systematically as follows. The angular momentum in a c-aniGTO basis set is usually limited to $a=10$ (m-type) in order to keep the size of the basis set within a reasonable limit. This corresponds to the highest vibrational quantum number v_{max} of 10 for a one-dimensional harmonic oscillator eigenfunction. The $\tilde{\omega}$ value may be determined as the value for which the energy of the highest state v_{max} of the harmonic oscillator, $\tilde{\omega}(v_{max}+\frac{1}{2})$, coincides with the energy of the $(v_{max}+1)$-th eigenstate of the one-dimensional Gaussian potential which is obtained by solving the one-dimensional Schrödinger equation numerically. In case the Gaussian potential supports only a smaller number of eigenstates than v_{max}, then, $\tilde{\omega}$ is chosen such that energy of the highest bound state, denoted as the Kth eigenstate, of the Gaussian potential coincides with the energy of the harmonic oscillator eigenstate with $v=K-1$.

TABLE I. Oscillator strengths for the $1\ ^1\Pi_u$-$1\ ^1\Sigma_g^+$ and $2\ ^1\Pi_u$-$1\ ^1\Sigma_g^+$ transitions of the two-electron Gaussian quantum dot with $(D,\omega,\omega_z)=(0.5,0.1,2.0)$ for different size basis sets.

	$1\ ^1\Pi_u$-$1\ ^1\Sigma_g^+$	$2\ ^1\Pi_u$-$1\ ^1\Sigma_g^+$
$1s1p1d1f1g$ (15)[a]	1.991	0.015
$1s1p1d1f1g1h$ (21)	1.968	0.030
$1s1p1d1f1g1h1i$ (28)	1.984	0.024
$1s1p1d1f1g1h1i1j$ (36)	1.974	0.029
$1s1p1d1f1g1h1i1j1k$ (45)	1.968	0.030
$1s1p1d1f1g1h1i1j1k1l$ (55)	1.968	0.029
$1s1p1d1f1g1h1i1j1k1l1m$ (66)	1.968	0.029

[a]The number in the round bracket indicates the total number of basis functions.

In order to check the reliability of the c-aniGTO basis set with respect to calculating oscillator strengths for electrons confined by the potential of Eq. (4) the oscillator strengths of the low-lying transitions of the singlet manifold of two electrons confined by the quasi-two-dimensional Gaussian potential with the parameters $(D,\omega,\omega_z)=(0.5,0.1,2.0)$ have been calculated for different size basis sets. The exponents of the c-aniGTO basis sets have been chosen to be half of $\tilde{\omega}$ for ζ_x and ζ_y and half of ω_z for ζ_z. Since ω_z is 20 times larger than ω only functions with $a_z=0$ have been selected and used in the basis sets.[35]

The oscillator strength for a transition from a low-lying state a to a high-lying state b with a transition dipole moment along the $\xi(=x,y,z)$ coordinate has been calculated as the product of the energy difference between the two electronic states and the square modulus of the matrix element of the transition moment along the ξ-axis as

$$T^{\xi}(b,a) = 2(E_b - E_a) \left| \langle \Psi_b | \sum_{i=1}^{N} \xi_i | \Psi_a \rangle \right|^2, \qquad (8)$$

where E_a and E_b represent the energies, Ψ_a and Ψ_b represent the corresponding CI wave functions, and ξ_i denotes the value of the ξ coordinate of the ith electron. In case the lower state a is degenerate due to spatial symmetry the oscillator strength of Eq. (8) is written as

$$T^{\xi}(b,a) = \frac{2(E_b - E_a)}{n_d} \sum_{d=1}^{n_d} \left| \langle \Psi_b | \sum_{i=1}^{N} \xi_i | \Psi_a^d \rangle \right|^2, \qquad (9)$$

where n_d denotes the degree of degeneracy and is always 2 in the present study. Since excitations occur in the low-energy region only along the x or y coordinate and the value of $T^{\xi}(b,a)$ is identical for the x and y coordinates for the isotropic Gaussian potential, the superscript ξ is omitted hereafter.

The results are summarized in Table I for the dipole-allowed $1\ ^1\Pi_u$-$1\ ^1\Sigma_g^+$ transition corresponding to the center-of-mass excitation and for the sideband $2\ ^1\Pi_u$-$1\ ^1\Sigma_g^+$ transition where the assignments of the states have been made by counting the states separately for each spatial and spin symmetry. As shown in Table I the oscillator strength for the

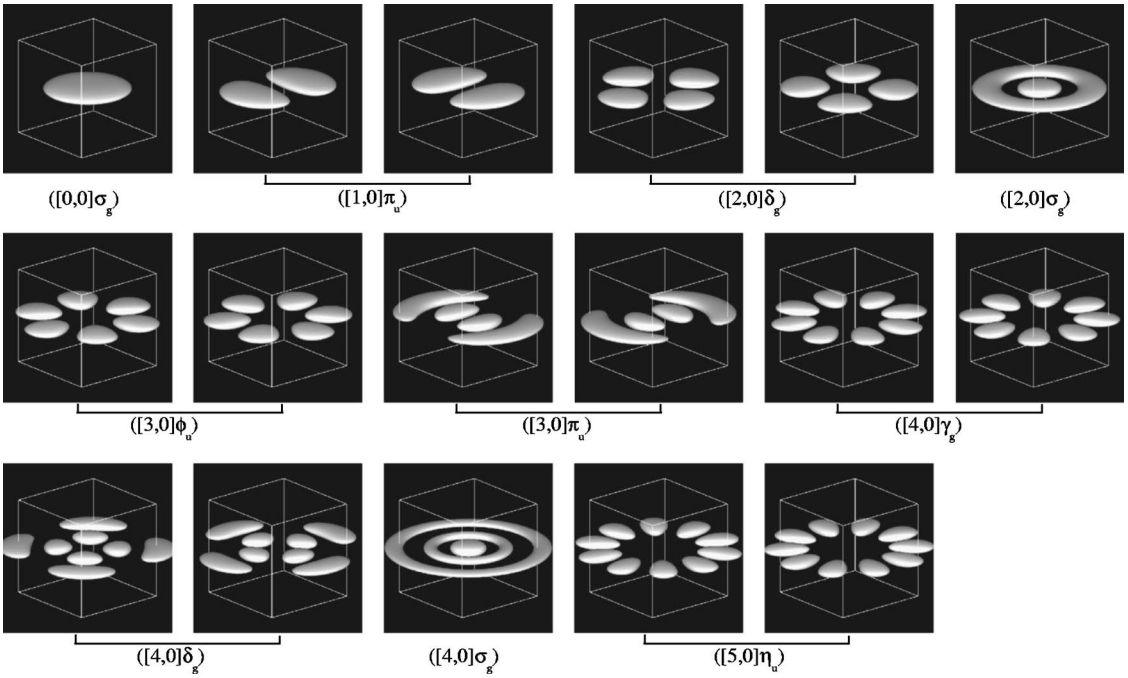

FIG. 2. The closed-shell Hartree-Hock orbital density distribution for two-electrons confined by a quasi-two-dimensional Gaussian potential with $(D,\omega,\omega_z)=(0.8,0.1,2.0)$. The side length of the cube is 16 a.u. The density at the surface is 1.0×10^{-3}.

$1\ ^1\Pi_u$-$1\ ^1\Sigma_g^+$ transition converges to the value of 1.968 within 0.001 for the basis sets equal to and larger than $[1s1p1d1f1g1h1i1j1k]$ of 45 functions. On the other hand, the oscillator strength for the $2\ ^1\Pi_u$-$1\ ^1\Sigma_g^+$ transition fluctuates between 0.030 and 0.029 and it finally converges to 0.029 for the largest basis set $[1s1p1d1f1g1h1i1j1k1l1m]$ of 66 functions. In order to study transitions with such small values of oscillator strengths the reduced basis set $[1s1p1d1f1g1h1i1j1k1l1m]$ of 66 functions is used in the present study. The results with this basis set are converged to five digits for the energies and to three digits for the oscillator strengths.

III. RESULTS AND DISCUSSION

A. Hartree-Fock orbitals

The closed-shell Hartree-Fock orbital density distributions for two-electrons confined by a quasi-two-dimensional Gaussian potential with $(D,\omega,\omega_z)=(0.8,0.1,2.0)$ have been calculated and are presented in Fig. 2. The density distribution is displayed in cubes with a side length of 16 a.u. The z axis is directed along the vertical edge of the cube. The density at the surface is 1.0×10^{-3}. It is noted that the nodal pattern of the orbital density distributions displayed in Fig. 2 are quite similar to those of quasi-two-dimensional harmonic oscillator quantum dots obtained in a previous study.[35] Therefore the same notation $[v_x+v_y,v_z]\Delta$ has been used to label the orbitals in Fig. 2 where v_x, v_y, and v_z denote one-electron harmonic-oscillator quantum numbers for the x, y, and z coordinates, respectively, and Δ denotes the symmetry labels of the $D_{\infty,h}$ group. The v_x and v_y quantum numbers are related to the quantum number of the z component of the angular momentum l_z and the number of *radial nodal planes* n by $l_z=v_x-v_y$ and $2n=v_x+v_y-|l_z|$, respectively, while the v_z quantum number is related to the number of nodal planes along the z axis that is always zero in the present study because of the strong confinement along the z direction.

As in the case of the quasi-two-dimensional harmonic oscillator quantum dots two types of *electron modes* are recognized in the nodal pattern of the Hartree-Fock orbitals displayed in Fig 2, namely, the *circular mode* with angular nodal planes and the *breathing mode* with radial nodal planes.[35] For example, the orbitals $[1,0]\pi_u$, $[2,0]\delta_g$, $[3,0]\phi_u$, etc., have one, two, and three angular nodal planes and therefore these orbitals have excitations into the circular mode with one, two, and three quanta, respectively. On the other hand, the orbitals $[2,0]\sigma_g$ and $[4,0]\sigma_g$ have one and two radial nodal planes, respectively, and therefore these orbitals have excitations into the breathing mode with one and two quanta, respectively. Besides these orbitals with the "overtone" excitations orbitals are present that have excitations into both the circular and breathing modes. For example, the $[3,0]\pi_u$ orbital has one angular nodal plane and one radial plane and the $[4,0]\delta_g$ orbital has two angular nodal planes and one radial nodal plane indicating that they are orbitals with "combinational" excitations.

It is convenient to address here the number of nodal planes for a given Hartree-Fock orbital. They are naturally defined by using the one-electron harmonic-oscillator quantum numbers v_x, v_y, and v_z as

$$v = v_x + v_y + v_z. \tag{10}$$

Since v_z is always zero in the present study v is written as the sum of angular nodal planes $|l_z|$ and radial nodal planes n

TABLE II. Ionization potential (in a.u.) of the quasi-two-dimensional Gaussian quantum dot with $\omega=0.1$ for different depth of the potential D.

	$2e$		$3e$		$4e$		
D	$1\,^1\Sigma_g^+$	$1\,^3\Pi_u$	$1\,^2\Pi_u$	$1\,^4\Sigma_g^-$	$1\,^1\Sigma_g^+$	$1\,^3\Sigma_g^-$	$1^5\Delta_g$
0.2							
0.3	0.0035						
0.4	0.0926	0.0665					
0.5	0.1865	0.1586	0.0083	0.0016			
0.6	0.2826	0.2535	0.0981	0.0912			
0.7	0.3798	0.3500	0.1911	0.1841	0.0543	0.0648	0.0274
0.8	0.4779	0.4474	0.2861	0.2790	0.1458	0.1568	0.1180
0.9	0.5763	0.5454	0.3823	0.3751	0.2394	0.2508	0.2109
1.0	0.6751	0.6438	0.4793	0.4720	0.3345	0.3461	0.3055

$$v = 2n + |l_z|. \tag{11}$$

In the following sections the total number of nodal planes in the multielectron wave functions have significant roles in analyzing the interaction among different electron modes.

B. Ionization potentials

Before discussing the oscillator strengths it should be noted that the quasi-two-dimensional Gaussian potential of Eq. (4) has a critical potential depth below which the electrons of the system are not bound because of the electron-electron repulsion interaction. This value depends on the strength of the confinement ω, the number of electrons, and the spin configuration of the systems. In order to determine how strongly electrons are bound for a given potential depth D the first ionization potentials have been calculated for the lowest energy states of all spin configurations of two, three, and four electrons confined by a potential with a small ($\omega=0.1$) and one with a large ($\omega=1.0$) strength of confinement. The ionization potential I_a^N for the state a with N electrons has been calculated by

$$I_a^N = E_g^{N-1} - E_a^N, \tag{12}$$

where E_a^N represent the energy of the state considered and E_g^{N-1} the ground-state energy of the system with $N-1$ electrons. The results are summarized in Tables II and III for $\omega=0.1$ and 1.0, respectively.

As shown in Tables II and III the first ionization potential becomes larger as the depth of the Gaussian potential D increases. The blanks shown in these tables indicate that the resultant ionization potential takes a negative value and therefore the system is unbound. The number of blanks increases in both tables as the number of electrons increases. It is noted that Table II representing the results for the smaller confinement strength $\omega=0.1$ has more blanks than Table III for the larger confinement strength $\omega=1.0$ although the range of the anharmonicity parameter α is the same in both cases $0.1\leqslant\alpha\leqslant0.5$. This indicates that the electron-electron interaction has a larger effect in the case of $\omega=0.1$ than of $\omega=1.0$. In order to compare the results for the smaller and the larger ω on the same ground the anharmonicity parameter $\alpha=0.125$ has been chosen for which all spin states listed in

TABLE III. Ionization potential (in a.u.) of the quasi-two-dimensional Gaussian quantum dot with $\omega=1.0$ for different depth of the potential D.

	$2e$		$3e$		$4e$		
D	$1\,^1\Sigma_g^+$	$1\,^3\Pi_u$	$1\,^2\Pi_u$	$1\,^4\Sigma_g^-$	$1\,^1\Sigma_g^+$	$1\,^3\Sigma_g^-$	$1^5\Delta_g$
2.0	0.3477						
3.0	1.2482	0.7523	0.1605				
4.0	2.2024	1.6626	1.0307	0.6368	0.4973	0.5780	
5.0	3.1755	2.6110	1.9585	1.5445	1.3988	1.4851	0.5455
6.0	4.1583	3.5775	2.9124	2.4848	2.3373	2.4267	1.4403
7.0	5.1458	4.5538	3.8800	3.4433	3.2945	3.3862	2.3696
8.0	6.1371	5.5364	4.8566	4.4123	4.2639	4.3568	3.3172
9.0	7.1304	6.5229	5.8385	5.3884	5.2404	5.3344	4.2772
10.0	8.1249	7.5122	6.8241	6.3695	6.2218	6.3166	5.2456

Tables II and III are bound. The effect of the electron-electron interaction on the distribution of oscillator strengths has been examined by focusing on the results with the same value of α, i.e., $(D,\omega)=(8.0,1.0)$ and (0.8, 0.1).

C. Oscillator strengths

1. Strongly confined electrons: Large ω

The distribution of oscillator strengths for transitions from the lowest states in all spin manifolds of two, three, and four electrons confined by the quasi-two-dimensional Gaussian potential with $(D,\omega,\omega_z)=(8.0,1.0,20.0)$ have been calculated and are displayed in Figs. 3(a)–3(g), respectively. In all these figures the horizontal axes represent the excitation energies from the lowest states and the dotted lines represent the oscillator strengths of the dipole-allowed transitions *in the harmonic limit*, that is, those of the quasi-two-dimensional harmonic oscillator quantum dot with $(\omega_x,\omega_y,\omega_z)=(1.0,1.0,20.0)$. As known from the $B=0$ case of the generalized Kohn theorem, where B represents the external magnetic field strength, the excitation energy is equal to the value of the strength of confinement $\omega(=\omega_x=\omega_y)$ of 1.0 and the oscillator strength is equal to the number of electrons.

As shown in Fig. 3(a) the distribution of oscillator strengths of the two-electron Gaussian quantum dot in the singlet manifold is concentrated almost exclusively in the $1\,^1\Pi_u$-$1\,^1\Sigma_g^+$ transition although a tiny peak is observed at $\Delta E=2.2420$ with an oscillator strength being as small as 0.0015. The excitation energy 0.9196 of the main peak is smaller than that of the corresponding harmonic limit of 1.0 due to the effect of anharmonicity of the Gaussian potential. The origin of this redshift can be understood easily from the one-dimensional Gaussian potential drawn in Fig. 1(b). When the confining potential becomes soft the energy level of each bound state is shifted to lower energies. Since this effect is larger for the higher-lying states than for the lower-lying states, the energy difference between the lowest state and an excited state becomes smaller than the corresponding value of the harmonic oscillator. The observed redshift may be specific to using a Gaussian confining potential. A blue-shift may be observed when the confining potential has the form of a harmonic-oscillator potential with a small hump at the center.[36,37]

In the case of the triplet manifold of the two-electron system shown in Fig. 3(b) the distribution of the oscillator strengths consists mainly of three peaks at $\Delta E=0.8545$, 0.8914, and 0.9309 corresponding to the $1\,^3\Sigma_g^+$-$1\,^3\Pi_u$, $1\,^3\Delta_g$-$1\,^3\Pi_u$, and $1\,^3\Sigma_g^-$-$1\,^3\Pi_u$ transitions, respectively. It is noted that in the harmonic limit the three states $1\,^3\Sigma_g^+$, $1\,^3\Delta_g$, and $1\,^3\Sigma_g^-$ become degenerate and merge into a single peak as displayed by the dotted line in Fig. 3(b). The summation of the oscillator strengths for these three transitions amounts to 1.998 indicating that the distribution of oscillator strengths is concentrated almost exclusively, like in the case of the singlet manifold, in the transitions corresponding to the dipole-allowed transitions in the harmonic limit.

In the case of three electrons the distribution of oscillator strengths displayed in Figs. 3(c) and 3(d) shows an additional structure that is not observed in the distribution of oscillator strength of two electrons. As shown in Fig. 3(c) the distribution of oscillator strengths in the doublet manifold is dominated, as for the triplet manifold of two electrons, by the close lying three peaks at $\Delta E=0.8714$, 0.8860, and 0.9119 corresponding to the $2\,^2\Sigma_g^+$-$1\,^2\Pi_u$, $2\,^2\Delta_g$-$1\,^2\Pi_u$, and $1\,^2\Sigma_g^-$-$1\,^2\Pi_u$ transitions, respectively, which merge into a single peak in the harmonic limit. However, it is noted that aside from these main peaks two sideband peaks are observed at $\Delta E=0.5822$ and 0.7378 corresponding to the $1\,^2\Delta_g$-$1\,^2\Pi_u$ and $1\,^2\Sigma_g^+$-$1\,^2\Pi_u$ transitions, respectively. In the case of the quartet manifold displayed in Fig. 3(d) the distribution of oscillator strengths consists also of a main peak and a sideband peak corresponding to the $2\,^4\Pi_u$-$1\,^4\Sigma_g^-$ and $1\,^4\Pi_u$-$1\,^4\Sigma_g^-$ transitions, respectively. Since a system of three electrons should have a larger density of states than a system of two electrons the oscillator strength of the dipole-allowed transition in the harmonic limit can be fragmented into the near lying transitions for three electrons which does not occur for two electrons owing to the sparse density of states.

The last statement is confirmed by the results for four electrons displayed in Figs. 3(e)–3(g). The distribution of oscillator strengths in the singlet manifold displayed in Fig. 3(e) has two main peaks corresponding to the $2\,^1\Pi_u$-$1\,^1\Delta_g$ and $1\,^1\Phi_u$-$1\,^1\Delta_g$ transitions and two sideband peaks corresponding to the $1\,^1\Pi_u$-$1\,^1\Delta_g$ and $3\,^3\Pi_u$-$1\,^1\Delta_g$ transitions. It is noted that the excitation energies of the two main peaks, $\Delta E=0.8584$ and 0.8605, are *accidentally* close to each other. In the case of the triplet manifold displayed in Fig. 3(f) the distribution of oscillator strengths consists of three peaks at $\Delta E=0.5408$, 0.7376, and 0.8674 corresponding to $1\,^3\Pi_u$-$1\,^3\Sigma_g^-$, $2\,^3\Pi_u$-$1\,^3\Sigma_g^-$, and $3\,^3\Pi_u$-$1\,^3\Sigma_g^-$ transitions, respectively. The first two transitions are the sideband transitions and the last corresponds to the dipole-allowed transition in the harmonic limit. In the case of the quintet manifold displayed in Fig. 3(g) the distribution of oscillator strengths, again, consists of main peaks and sideband peaks. The $1\,^5\Phi_u$-$1\,^5\Delta_g$ and $2\,^5\Pi_u$-$1\,^5\Delta_g$ transitions at $\Delta E=0.8346$ and 0.8575 correspond to the dipole-allowed transitions in the harmonic limit. The other peaks at $\Delta E=0.7514$ and 0.8883, assigned as the $1\,^5\Pi_u$-$1\,^5\Delta_g$ and $3\,^5\Pi_u$-$1\,^5\Delta_g$ transitions, respectively, are the sideband transitions. In all spin manifolds of four electrons the distribution of oscillator strengths consists of main peaks and sideband peaks as observed for the three-electron case.

2. Weakly confined electrons: Small ω

The distribution of oscillator strengths becomes significantly more complicated when the strength of confinement becomes small. The distribution of oscillator strengths for the same transitions discussed in the last section for two, three, and four electrons confined by a Gaussian potential with $(D,\omega,\omega_z)=(0.8,0.1,2.0)$ has been calculated and are displayed in Figs. 4(a)–4(g), respectively. The potential has the same anharmonicity but the strength of confinement is ten times smaller. In all these figures the horizontal axes represent the excitation energies from the lowest states and the dotted lines represent the oscillator strengths of the dipole-allowed transitions in the harmonic limit.

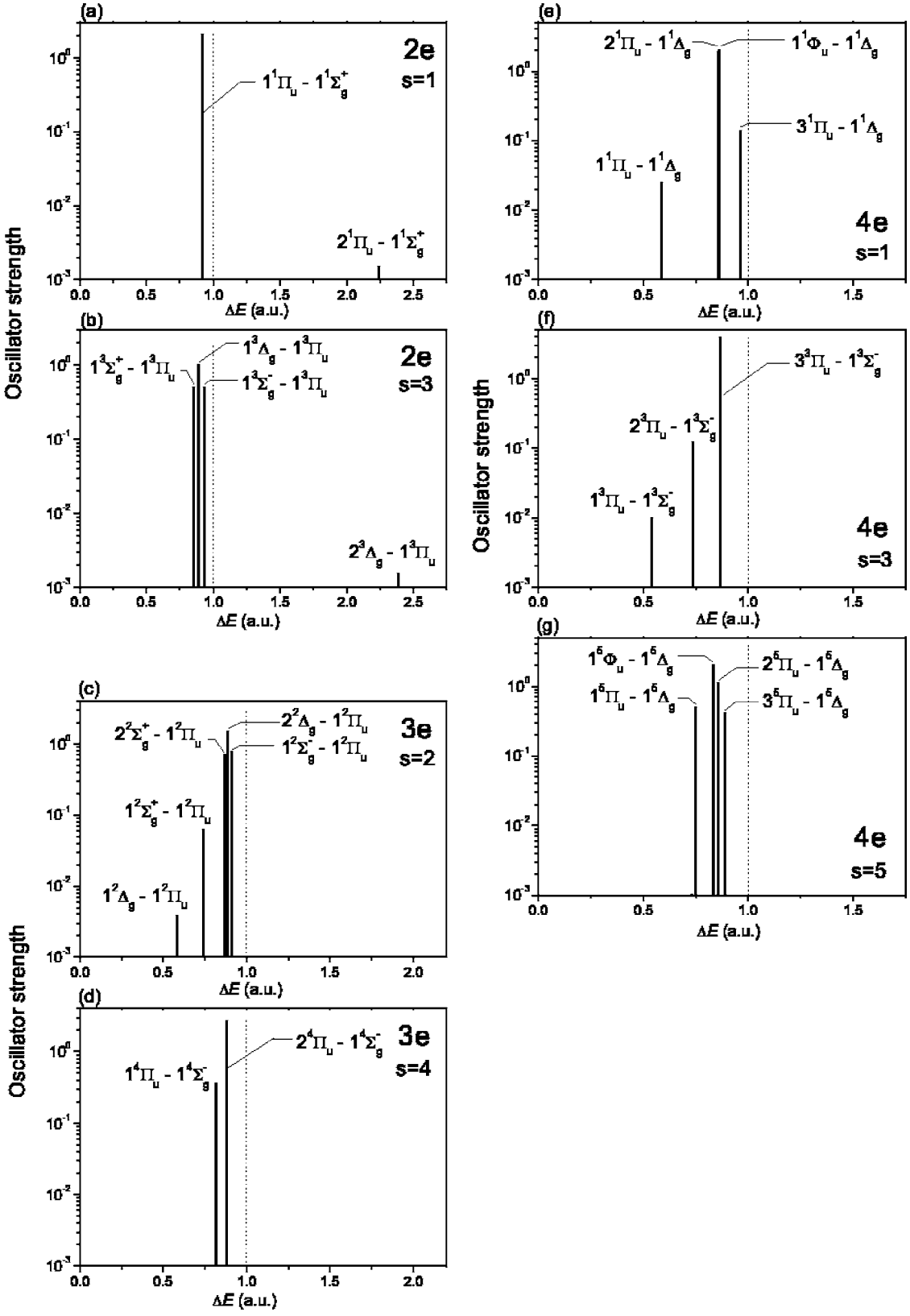

FIG. 3. Distribution of oscillator strengths from the lowest state in each spin manifold of two, three, and four electrons confined by a quasi-two-dimensional Gaussian potential with $(D,\omega,\omega_z)=(8.0,1.0,20.0)$. The horizontal axis represents the excitation energy. The dotted line represents the oscillator strength of the dipole-allowed transition in the harmonic limit, i.e., $D=\infty$.

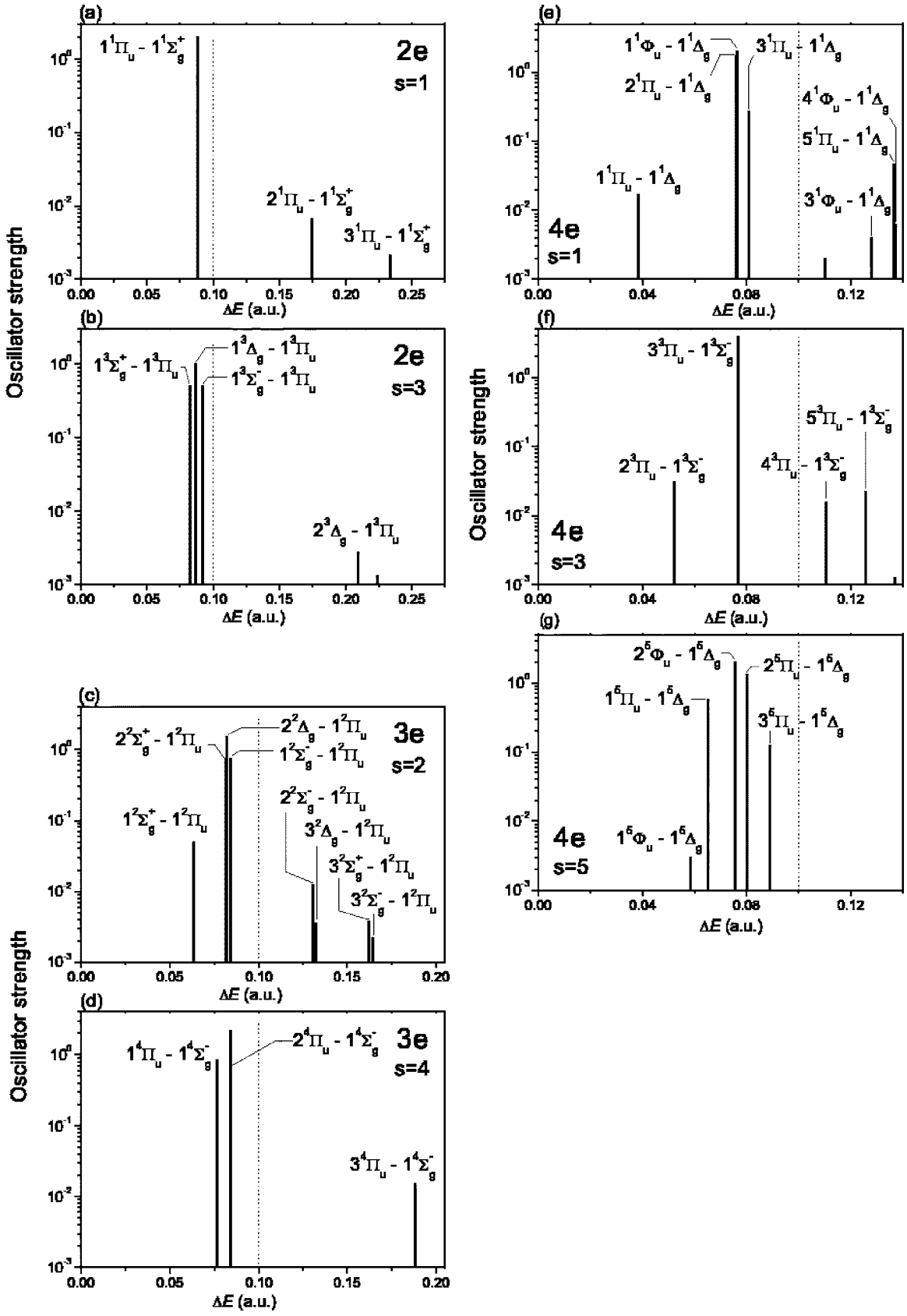

FIG. 4. Distribution of oscillator strengths from the lowest state in each spin manifold of two, three, and four electrons confined by a quasi-two-dimensional Gaussian potential with $(D,\omega,\omega_z)=(0.8,0.1,2.0)$. See Fig. 3 for other remarks.

The result for two electrons in the singlet manifold displayed in Fig. 4(a) has some similarity with the corresponding result for large ω displayed in Fig. 3(a) in that the main peak at $\Delta E=0.08836$ corresponds to the $1\,^1\Pi_u$-$1\,^1\Sigma_g^+$ transition. However, it is noted that the distribution displayed in Fig. 4(a) shows two additional peaks in the higher energy region at $\Delta E=0.1744$ and 0.2334 while the distribution for large ω displayed in Fig. 3(a) shows only a tiny peak as discussed in the previous section. A similar observation is made for the triplet manifold displayed in Fig. 4(b) where aside from the three main peaks an additional peak assigned as the $2\,^3\Delta_g$-$1\,^3\Pi_u$ transition is observed in the higher energy region at $\Delta E=0.2096$.

In the case of three and four electrons the distribution of oscillator strengths has a rich structure as displayed in Fig. 4(c)–4(g). The result for three electrons in the doublet manifold displayed in Fig. 4(c) shows two pairs of doublets appearing in the high energy region at about $\Delta E=0.13$ and 0.16 in addition to the three main peaks and a sideband peak, $1\,^2\Sigma_g^+$-$1\,^2\Pi_u$, for large ω as displayed in Fig. 3(c). It is noted that the other sideband peak in the low energy region, $1\,^2\Delta_g$-$1\,^2\Pi_u$, which has been observed for large ω displayed in Fig. 3(c) can hardly be observed in Fig. 4(c). This indicates that for small ω the oscillator strength for this $1\,^2\Delta_g$-$1\,^2\Pi_u$ transition has been "used" for the new transitions in the high energy region. As for the doublet manifold the distribution of oscillator strengths in the quartet manifold has an additional peak in the high energy region at $\Delta E=0.1886$ as displayed in Fig. 4(c). It is noticed in Figs. 4(c) and 4(d) that the distribution of the quartet manifold is simpler than that of the doublet manifold. This is due to the fact that in the quartet manifold only Π states are accessible from the lowest $1\,^4\Sigma_g^-$ state while in the doublet manifold both Σ and Δ states are accessible from the lowest $1\,^2\Pi_u$ state.

A comparison of Figs. 3 and 4 for four electrons shows that observations similar to those for the two- and three-electron case can be made for the four-electron case: The oscillator strengths for the transitions to higher-lying states which can hardly be observed for large ω acquire a certain intensity for small ω. The results for the singlet and triplet manifolds show a number of states appearing as displayed in Figs. 4(e) and 4(f). In the case of the quintet manifold no transitions are observed in the high energy range displayed in Fig. 4(g) but there exists a transition, $4\,^5\Pi_u$-$1\,^5\Delta_g$, in the higher energy region at $\Delta E=0.1634$. Except for this transition all transitions with oscillator strengths larger than 1.0×10^{-3} have been displayed in the figures.

3. Interpretation: Effect of electron-electron interaction

The observations made in the last two sections show that the number of excitations into higher-lying states is increased when the strength of confinement becomes small. Since the anharmonicity parameter α is the same for the two cases of large and small ω, that is, the shape of the confining potential is the same in both cases, the observed differences must be ascribed to the difference in the relative importance of the electron-electron interaction. Therefore it can be said that the energy absorbed from a radiation field by the center-of-mass mode can be more efficiently redistributed internally for small ω than for large ω through the electron-electron interaction.

In order to understand the internal energy redistribution the leading configurations and their weights defined by the square norm of the coefficients in the CI wave functions for the states displayed in Fig. 3 for large ω and in Fig. 4 for small ω have been examined and listed in Tables IV and V, respectively. The configurations are represented in terms of the notations defined for the Hartree-Fock orbitals in Sec. III A. The states with an asterisk at the head of the state-label are the lowest states for the corresponding spin manifold. The *polyad quantum number* denoted as υ_p that characterizes the configurations is also listed in Tables IV and V. It is defined as the number of nodal planes summed over all Hartree-Fock orbitals involved in the leading configuration. As has been reported in previous studies on anisotropic harmonic-oscillator quantum dots[27,35] the square-norm of the leading configurations represented in Tables IV and V are usually smaller for the smaller confinement strength due to a larger configuration mixing.

The radiative transitions discussed in the last two sections can be interpreted consistently by using the leading configurations listed in Tables IV and V. In case of the $1\,^1\Pi_u$-$1\,^1\Sigma_g^+$ transition of two electrons displayed in Fig. 3(a), for example, the lower $1\,^1\Sigma_g^+$ state and the higher $1\,^1\Pi_u$ state have the configuration of $([0,0]\sigma_g)^2$ and $([0,0]\sigma_g)([1,0]\pi_u)$, respectively. Therefore this transition is interpreted as a one-electron excitation from the lowest $[0,0]\sigma_g$ orbital to the $[1,0]\pi_u$ orbital. In the case of the triplet manifold of two electrons displayed in Fig. 3(b) the four states $1\,^3\Pi_u$, $1\,^3\Sigma_g^+$, $1\,^3\Delta_g$, and $1\,^3\Sigma_g^-$ are involved in the displayed three transitions. They have the leading configurations $([0,0]\sigma_g)([1,0]\pi_u)$, $([0,0]\sigma_g)([2,0]\sigma_g)$, $([0,0]\sigma_g)([2,0]\delta_g)$, and $([1,0]\pi_u)([1,0]\pi_u)$, respectively. Therefore the $1\,^3\Sigma_g^+$-$1\,^3\Pi_u$ transition is a one-electron excitation from $[1,0]\pi_u$ to $[2,0]\sigma_g$, the $1\,^3\Delta_g$-$1\,^3\Pi_u$ transition is a one-electron excitation from $[1,0]\pi_u$ to $[2,0]\delta_g$, and the $1\,^3\Sigma_g^-$-$1\,^3\Pi_u$ transition is a one-electron excitation from $[0,0]\sigma_g$ to $[1,0]\pi_u$, and so on.

According to the analysis of the leading configurations all these states can be classified into sets of groups, each of which is characterized by a different value of the polyad quantum number defined previously as the number of nodal planes summed over all Hartree-Fock orbitals involved in the leading configuration. The number of nodal planes for each orbital is equal to the value of $\upsilon_x+\upsilon_y$ as defined in Sec. III A. For example, the leading configuration of the $3\,^5\Pi_u$ state of four electrons listed at the bottom of Table IV consists of the four orbitals $([0,0]\sigma_g)$, $([1,0]\pi_u)$, $([2,0]\delta_g)$, and $([2,0]\sigma_g)$ having 0, 1, 2, and 2 nodal planes, respectively, summing to $\upsilon_p=5$. The idea of polyads has a long history in molecular vibrational spectroscopy[38,39] and has been used for assigning vibrational states of polyatomic molecules when it is difficult to specify all *normal-mode* vibrational quantum numbers owing to prevalence of anharmonic coupling among the normal modes.[40–43] In this case, instead of assigning a set of

TABLE IV. Leading configurations, their weights, and polyad quantum numbers v_p for low-lying states of the two, three, and four electrons confined by the quasi-two-dimensional Gaussian potential with $(D,\omega,\omega_z)=(8.0,1.0,20.0)$. The state with an asterisk at the head of state label is the lowest state for the corresponding spin manifold.

	State	Configuration	Weight	v_p
$2e$	$^*1\ ^1\Sigma_g^+$	$([0,0]\sigma_g)^2$	0.97	0
	$1\ ^1\Pi_u$	$([0,0]\sigma_g)([1,0]\pi_u)$	0.96	1
	$^*1\ ^3\Pi_u$	$([0,0]\sigma_g)([1,0]\pi_u)$	0.98	1
	$1\ ^3\Sigma_g^+$	$([0,0]\sigma_g)([2,0]\sigma_g)$	0.97	2
	$1\ ^3\Delta_g$	$([0,0]\sigma_g)([2,0]\delta_g)$	0.98	2
	$1\ ^3\Sigma_g^-$	$([1,0]\pi_u)([1,0]\pi_u)$	0.97	2
$3e$	$^*1\ ^2\Pi_u$	$([0,0]\sigma_g)^2([1,0]\pi_u)$	0.95	1
	$1\ ^2\Delta_g$	$([0,0]\sigma_g)([1,0]\pi_u)^2$	0.60	2
	$1\ ^2\Sigma_g^+$	$([0,0]\sigma_g)^2([2,0]\sigma_g)$	0.59	2
	$2\ ^2\Sigma_g^+$	$([0,0]\sigma_g)([1,0]\pi_u)^2$	0.57	2
	$2\ ^2\Delta_g$	$([0,0]\sigma_g)^2([2,0]\delta_g)$	0.58	2
	$1\ ^2\Sigma_g^-$	$([0,0]\sigma_g)([1,0]\pi_u)([1,0]\pi_u)$	0.94	2
	$^*1\ ^4\Sigma_g^-$	$([0,0]\sigma_g)([1,0]\pi_u)([1,0]\pi_u)$	0.98	2
	$1\ ^4\Pi_u$	$([0,0]\sigma_g)([1,0]\pi_u)([2,0]\sigma_g)$	0.92	3
	$2\ ^4\Pi_u$	$([0,0]\sigma_g)([1,0]\pi_u)([2,0]\delta_g)$	0.91	3
$4e$	$^*1\ ^1\Delta_g$	$([0,0]\sigma_g)^2([1,0]\pi_u)^2$	0.91	2
	$1\ ^1\Pi_u$	$([0,0]\sigma_g)^2([1,0]\pi_u)([2,0]\delta_g)$	0.46	3
	$2\ ^1\Pi_u$	$([0,0]\sigma_g)^2([1,0]\pi_u)([2,0]\sigma_g)$	0.51	3
	$1\ ^1\Phi_u$	$([0,0]\sigma_g)^2([1,0]\pi_u)([2,0]\delta_g)$	0.89	3
	$3\ ^1\Pi_u$	$([0,0]\sigma_g)([1,0]\pi_u)^2([1,0]\pi_u)$	0.40	3
	$^*1\ ^3\Sigma_g^-$	$([0,0]\sigma_g)^2([1,0]\pi_u)([1,0]\pi_u)$	0.93	2
	$1\ ^3\Pi_u$	$([0,0]\sigma_g)([1,0]\pi_u)^2([1,0]\pi_u)$	0.63	3
	$2\ ^3\Pi_u$	$([0,0]\sigma_g)^2([1,0]\pi_u)([2,0]\sigma_g)$	0.80	3
	$3\ ^3\Pi_u$	$([0,0]\sigma_g)^2([1,0]\pi_u)([2,0]\delta_g)$	0.51	3
	$^*1\ ^5\Delta_g$	$([0,0]\sigma_g)([1,0]\pi_u)([1,0]\pi_u)([2,0]\delta_g)$	0.98	4
	$1\ ^5\Pi_u$	$([0,0]\sigma_g)([1,0]\pi_u)([1,0]\pi_u)([3,0]\pi_u)$	0.75	5
	$1\ ^5\Phi_u$	$([0,0]\sigma_g)([1,0]\pi_u)([1,0]\pi_u)([3,0]\phi_u)$	0.73	5
	$2\ ^5\Pi_u$	$([0,0]\sigma_g)([1,0]\pi_u)([2,0]\delta_g)([2,0]\delta_g)$	0.86	5
	$3\ ^5\Pi_u$	$([0,0]\sigma_g)([1,0]\pi_u)([2,0]\delta_g)([2,0]\sigma_g)$	0.77	5

quantum numbers to each vibrational state a group of states is assigned simultaneously by a polyad quantum number.

As shown in Table IV representing the result for large ω all states in each spin manifold have the same polyad quantum number v_p except the lowest state for which v_p is smaller by one quantum. For example, in the case of the doublet manifold of three electrons the lowest $1\ ^2\Pi_u$ state has a polyad quantum number of $v_p=1$ while all five excited states $1\ ^2\Delta_g$, $1\ ^2\Sigma_g^+$, $2\ ^2\Sigma_g^+$, $2\ ^2\Delta_g$, and $1\ ^2\Sigma_g^-$, have the polyad quantum number $v_p=2$. This observation indicates that the photon energy absorbed by the lowest state generates the center-of-mass excited states by creating one nodal plane in the lowest state. The absorbed energy is then transferred from the CM excited states to the states with the same value of v_p. In the above example of the doublet manifold of three electrons the radiation field excites the lowest $1\ ^2\Pi_u$ state into the three center-of-mass excited states $2\ ^2\Sigma_g^+$, $2\ ^2\Delta_g$, and $1\ ^2\Sigma_g^-$ and subsequently the two states $1\ ^2\Delta_g$ and $1\ ^2\Sigma_g^\pm$ with the same v_p and the same symmetry as the corresponding CM excited state are excited.

On the other hand, in the case of small $\omega=0.1$ listed in Table V *three* different values of v_p are observed for each spin manifold: a value for the lowest state, a value for the center-of-mass excited states and for states close to them, and a value for higher-lying states that is greater by two than the value of the CM excited states. For example, in case of the doublet manifold of three electrons the value of v_p for the lowest state and for the four excited states including the CM excited states is 1 and 2, respectively, as for large ω. But the additional four states $2\ ^2\Sigma_g^-$, $3\ ^2\Delta_g$, $3\ ^2\Sigma_g^+$, and $3\ ^2\Sigma_g^-$ have a value of $v_p=4$. It is noted that states with a polyad quantum number larger by one quantum than the values for the center-of-mass excited states cannot be coupled to the CM excited states and therefore cannot be excited since such states must have a different spatial symmetry. These observations indicate that for the case $\omega=0.1$ the energy absorbed from the

TABLE V. Leading configurations, their weights, and polyad quantum numbers v_p for low-lying states of the two, three, and four electrons confined by the quasi-two-dimensional Gaussian potential with $(D,\omega,\omega_z)=(0.8,0.1,2.0)$. The state with an asterisk at the head of state label is the lowest state for the corresponding spin manifold.

	State	Configuration	Weight	v_p
$2e$	$^*1\ ^1\Sigma_g^+$	$([0,0]\sigma_g)^2$	0.84	0
	$1\ ^1\Pi_u$	$([0,0]\sigma_g)([1,0]\pi_u)$	0.76	1
	$2\ ^1\Pi_u$	$([1,0]\pi_u)([2,0]\sigma_g)$	0.31	3
	$3\ ^1\Pi_u$	$([0,0]\sigma_g)([3,0]\pi_u)$	0.54	3
	$^*1\ ^3\Pi_u$	$([0,0]\sigma_g)([1,0]\pi_u)$	0.86	1
	$1\ ^3\Sigma_g^+$	$([0,0]\sigma_g)([2,0]\sigma_g)$	0.80	2
	$1\ ^3\Delta_g$	$([0,0]\sigma_g)([2,0]\delta_g)$	0.82	2
	$1\ ^3\Sigma_g^-$	$([1,0]\pi_u)([1,0]\pi_u)$	0.77	2
	$2\ ^3\Delta_g$	$([0,0]\sigma_g)([4,0]\delta_g)$	0.28	4
$3e$	$^*1\ ^2\Pi_u$	$([0,0]\sigma_g)^2([1,0]\pi_u)$	0.70	1
	$1\ ^2\Sigma_g^+$	$([0,0]\sigma_g)^2([2,0]\sigma_g)$	0.43	2
	$2\ ^2\Sigma_g^+$	$([0,0]\sigma_g)([1,0]\pi_u)^2$	0.37	2
	$2\ ^2\Delta_g$	$([0,0]\sigma_g)^2([2,0]\delta_g)$	0.43	2
	$1\ ^2\Sigma_g^-$	$([0,0]\sigma_g)([1,0]\pi_u)([1,0]\pi_u)$	0.63	2
	$2\ ^2\Sigma_g^-$	$([0,0]\sigma_g)([2,0]\delta_g)([2,0]\delta_g)$	0.16	4
	$3\ ^2\Delta_g$	$([0,0]\sigma_g)([2,0]\delta_g)([2,0]\sigma_g)$	0.22	4
	$3\ ^2\Sigma_g^+$	$([0,0]\sigma_g)([2,0]\sigma_g)^2$	0.26	4
	$3\ ^2\Sigma_g^-$	$([0,0]\sigma_g)([1,0]\pi_u)([3,0]\pi_u)$	0.44	4
	$^*1\ ^4\Sigma_g^-$	$([0,0]\sigma_g)([1,0]\pi_u)([1,0]\pi_u)$	0.88	2
	$1\ ^4\Pi_u$	$([0,0]\sigma_g)([1,0]\pi_u)([2,0]\sigma_g)$	0.85	3
	$2\ ^4\Pi_u$	$([0,0]\sigma_g)([1,0]\pi_u)([2,0]\delta_g)$	0.84	3
	$3\ ^4\Pi_u$	$([0,0]\sigma_g)([1,0]\pi_u)([4,0]\delta_g)$	0.33	5
$4e$	$^*1\ ^1\Delta_g$	$([0,0]\sigma_g)^2([1,0]\pi_u)^2$	0.56	2
	$1\ ^1\Pi_u$	$([0,0]\sigma_g)^2([1,0]\pi_u)([2,0]\delta_g)$	0.34	3
	$2\ ^1\Pi_u$	$([0,0]\sigma_g)^2([1,0]\pi_u)([2,0]\sigma_g)$	0.32	3
	$1\ ^1\Phi_u$	$([0,0]\sigma_g)^2([1,0]\pi_u)([2,0]\delta_g)$	0.50	3
	$3\ ^1\Pi_u$	$([0,0]\sigma_g)([1,0]\pi_u)^2([1,0]\pi_u)$	0.21	3
	$3\ ^1\Phi_u$	$([0,0]\sigma_g)^2([1,0]\pi_u)([4,0]\gamma_g)$	0.23	5
	$5\ ^1\Pi_u$	$([0,0]\sigma_g)^2([1,0]\pi_u)([4,0]\sigma_g)$	0.15	5
	$4\ ^1\Phi_u$	$([1,0]\pi_u)([1,0]\pi_u)^2([2,0]\delta_g)$	0.16	5
	$^*1\ ^3\Sigma_g^-$	$([0,0]\sigma_g)^2([1,0]\pi_u)([1,0]\pi_u)$	0.62	2
	$2\ ^3\Pi_u$	$([0,0]\sigma_g)^2([1,0]\pi_u)([2,0]\sigma_g)$	0.45	3
	$3\ ^3\Pi_u$	$([0,0]\sigma_g)^2([1,0]\pi_u)([2,0]\delta_g)$	0.29	3
	$4\ ^3\Pi_u$	$([0,0]\sigma_g)^2([1,0]\pi_u)([1,0]\pi_u)([3,0]\pi_u)$	0.12	5
	$5\ ^3\Pi_u$	$([0,0]\sigma_g)^2([1,0]\pi_u)([2,0]\delta_g)([2,0]\delta_g)$	0.11	5
	$^*1\ ^5\Delta_g$	$([0,0]\sigma_g)([1,0]\pi_u)([1,0]\pi_u)([2,0]\delta_g)$	0.87	4
	$1\ ^5\Phi_u$	$([0,0]\sigma_g)([1,0]\pi_u)([2,0]\delta_g)([2,0]\sigma_g)$	0.38	5
	$1\ ^5\Pi_u$	$([0,0]\sigma_g)([1,0]\pi_u)([1,0]\pi_u)([3,0]\pi_u)$	0.59	5
	$2\ ^5\Phi_u$	$([0,0]\sigma_g)([1,0]\pi_u)([1,0]\pi_u)([3,0]\phi_u)$	0.59	5
	$2\ ^5\Pi_u$	$([0,0]\sigma_g)([1,0]\pi_u)([2,0]\delta_g)([2,0]\delta_g)$	0.69	5
	$3\ ^5\Pi_u$	$([0,0]\sigma_g)([1,0]\pi_u)([2,0]\delta_g)([2,0]\sigma_g)$	0.38	5

radiation field is not only distributed among the states with $v_p=v_{p,cm}$, i.e., within the same polyad as the center-of-mass excited states but also transferred to states with $v_p=v_{p,cm}+2$. Since the electron-electron interaction plays a more important role in the case of small ω than in the case of large ω the electron-electron interaction appears to promote the *inter-polyad* energy transfer between the states with $v_p=v_{p,cm}$ and those with $v_p=v_{p,cm}+2$. When the strength of

confinement becomes even smaller the inter-polyad mixing becomes stronger which may eventually break the polyad structure and lead to so-called quantum chaotic states.[44–46]

IV. SUMMARY

In the present study the energy spectra and oscillator strengths of two, three, and four electrons confined by a quasi-two-dimensional Gaussian potential have been calculated for different strength of confinement ω and potential depth D by using the quantum chemical configuration interaction method employing reduced Cartesian anisotropic Gaussian basis sets. An optimum basis set has been constructed by checking the convergence of the calculated oscillator strengths.

The first ionization potential has been calculated for $\omega=1.0$ and 0.1 by changing the potential depth D in order to identify the critical potential depth with which all electrons of the system can be bound. A substantial redshift has been observed for the transitions corresponding to the excitation into the center-of-mass mode. The oscillator strengths, concentrated exclusively in the center-of-mass excitation in the harmonic limit, are distributed among the near-lying transitions. It is shown that the distribution of the oscillator strengths is limited to transitions located in the lower-energy region for $\omega=1.0$ but extends towards the higher-energy region for $\omega=0.1$. The analysis of the leading configurations in the CI wave functions shows that all states studied can be classified according to the value of the polyad quantum number v_p defined as the number of nodal planes summed over all one-particle Hartree-Fock orbitals in the configuration. It is shown that the distribution of the oscillator strengths for larger ω occurs among transitions involving excited states with the same polyad quantum number v_p as the center-of-mass-mode excited state, $v_{p,cm}$, while for the smaller ω it occurs among transitions involving excited states with $v_p=v_{p,cm}$ and $v_p=v_{p,cm}+2$. The existence of a polyad structure in the anharmonic quantum dots could be useful in making assignments for experimental optical absorption spectra.

ACKNOWLEDGMENTS

The present study has been supported in part by the Grants-in-Aid for Scientific Research (No. 16750007) from the Ministry of Education, Science, Sports and Culture and by the fund from the Matsuo Foundation. T.S. thanks the Alexander von Humboldt Foundation. P.A.H. also thanks the Nihon University.

*Electronic address: sako@phys.ge.cst.nihon-u.ac.jp
†Electronic address: ghd@mpa-garching.mpg.de; URL: http://www.mpa-garching.mpg.de/mol_physics/index.shtml

[1] R. C. Ashoori, Nature (London) **379**, 413 (1996).
[2] N. F. Johnson, J. Phys.: Condens. Matter **7**, 965 (1995).
[3] S. Tarucha, D. G. Austing, T. Honda, R. J. van der Hage, and L. P. Kouwenhoven, Phys. Rev. Lett. **77**, 3613 (1996).
[4] L. Kouwenhoven, T. H. Oosterkamp, M. W. S. Danoesastro, M. Eto, D. G. Austing, T. Honda, and S. Tarucha, Science **278**, 1788 (1997).
[5] P. Matagne, J. P. Leburton, D. G. Austing, and S. Tarucha, Physica E (Amsterdam) **13**, 679 (2002).
[6] P. A. Maksym and T. Chakraborty, Phys. Rev. Lett. **65**, 108 (1990).
[7] U. Merkt, J. Huser, and M. Wagner, Phys. Rev. B **43**, 7320 (1991).
[8] W. Kohn, Phys. Rev. **123**, 1242 (1961).
[9] L. Brey, N. F. Johnson, and B. I. Halperin, Phys. Rev. B **40**, 10647 (1989).
[10] F. M. Peeters, Phys. Rev. B **42**, 1486 (1990).
[11] Q. P. Li, K. Karräi, S. K. Yip, S. D. Sarma, and H. D. Drew, Phys. Rev. B **43**, 5151 (1991).
[12] J. F. Dobson, Phys. Rev. Lett. **73**, 2244 (1994).
[13] M. Pi, F. Ancilotto, E. Lipparini, and R. Mayol, Physica E (Amsterdam) **24**, 297 (2004).
[14] P. Matagne and J. P. Leburton, Phys. Rev. B **65**, 235323 (2002).
[15] D. Pfannkuche and R. R. Gerhardts, Phys. Rev. B **44**, 13132 (1991).
[16] X. C. Xie, S. Das Sarma, and S. He, Phys. Rev. B **48**, 8454 (1993).
[17] D. Heitmann, K. Bollweg, V. Gudmundsson, T. Kurth, and S. P. Riege, Physica E (Amsterdam) **1**, 204 (1997).
[18] I. Magnúsdóttir and V. Gudmundsson, Phys. Rev. B **60**, 16591 (1999).
[19] J. Adamowski, M. Sobkowicz, B. Szafran, and S. Bednarek, Phys. Rev. B **62**, 4234 (2000).
[20] G. H. F. Diercksen and G. G. Hall, Comput. Phys. **8**, 215 (1994).
[21] L. Laaksonen, J. Mol. Graphics **10**, 33 (1992).
[22] D. L. Bergman, L. Laaksonen, and A. Laaksonen, J. Mol. Graphics Modell. **15**, 301 (1997).
[23] M. Wagner, U. Merkt, and A. V. Chaplik, Phys. Rev. B **45**, 1951 (1992).
[24] J. T. Lin and T. F. Jiang, Phys. Rev. B **64**, 195323 (2001).
[25] T. Sako and G. H. F. Diercksen, J. Phys. B **36**, 1433 (2003).
[26] T. Sako and G. H. F. Diercksen, J. Phys. B **36**, 1681 (2003).
[27] T. Sako and G. H. F. Diercksen, J. Phys.: Condens. Matter **15**, 5487 (2003).
[28] W. Becken, P. Schmelcher, and F. K. Diakonos, J. Phys. B **32**, 1557 (1999).
[29] W. Becken and P. Schmelcher, J. Phys. B **33**, 545 (2000).
[30] M. Braskén, M. Lindberg, D. Sundholm, and J. Olsen, Phys. Rev. B **61**, 7652 (2000).
[31] S. Corni, M. Braskén, M. Lindberg, J. Olsen, and D. Sundholm, Phys. Rev. B **67**, 085314 (2003).
[32] O. Dippel, P. Schmelcher, and L. S. Cederbaum, Phys. Rev. A **49**, 4415 (1994).
[33] P. S. Drouvelis, P. Schmelcher, and F. K. Diakonos, J. Phys.: Condens. Matter **16**, 3633 (2004).
[34] P. S. Drouvelis, P. Schmelcher, and F. K. Diakonos, Phys. Rev. B **69**, 035333 (2004).

[35] T. Sako and G. H. F. Diercksen, J. Phys.: Condens. Matter **17**, 5159 (2005).
[36] J. B. Coon, N. W. Naugle, and R. Mackenzie, J. Mol. Spectrosc. **20**, 107 (1966).
[37] T. Sako, A. Hishikawa, and K. Yamanouchi, Chem. Phys. Lett. **294**, 571 (1998).
[38] W. Low, Phys. Rev. **97**, 1664 (1955).
[39] G. D. Saksena, T. A. Wiggins, and D. H. Rank, J. Chem. Phys. **31**, 839 (1959).
[40] M. E. Kellman and E. D. Lynch, J. Chem. Phys. **85**, 7216 (1986).
[41] L. Xiao and M. E. Kellman, J. Chem. Phys. **90**, 6086 (1989).
[42] M. A. Temsamani, M. Herman, S. A. B. Solina, J. P. O'Brien, and R. W. Field, J. Chem. Phys. **105**, 11357 (1996).
[43] T. Sako, K. Yamanouchi, and F. Iachello, J. Chem. Phys. **117**, 1641 (2002).
[44] R. Fleischmann, T. Geisel, and R. Ketzmerick, Phys. Rev. Lett. **68**, 1367 (1992).
[45] H. Bruus and A. D. Stone, Phys. Rev. B **50**, 18275 (1994).
[46] Y. H. Kim, M. Barth, H. J. Stöckmann, and J. P. Bird, Phys. Rev. B **65**, 165317 (2002).